interesting alternative is that phase-shifted intensities of each pixel at different time instances are recorded at four neighboring pixels at the same time instance.[60] These variations are called the spatial phase-shifting (SPS) technique.

1.4 Fourier Transform Technique

Another fundamental and successful technique for phase extraction is to introduce a spatial carrier into a fringe pattern, followed by a Fourier transform. The carrier can be introduced by simply tilting the mirror reflecting the reference beam. This technique was originally proposed for each line of a fringe pattern and is thus 1D.[61,62] It was also used for 1D temporal data.[63] The algorithm was later extended to 2D[64] and 3D.[65] An overview of the technique can be found in Ref. 66. The 2D case is used here for explanation.

The Fourier transform is an important harmonic analysis tool.[43,44] A 1D forward and inverse Fourier transform pair is defined as

$$Ff(\xi_x) = \int_{-\infty}^{\infty} f(x)\exp(-j\xi_x x)dx, \tag{1.28}$$

$$f(x) = \frac{1}{2\pi}\int_{-\infty}^{\infty} Ff(\xi_x)\exp(j\xi_x x)d\xi_x, \tag{1.29}$$

where $Ff(\xi_x)$ is the Fourier transform (or Fourier spectrum) of $f(x)$, and ξ_x is the frequency coordinate in the Fourier domain. For temporal data, we simply replace x and ξ_x with t and ξ_t, respectively. A 2D Fourier transform pair is similarly defined as follows:

$$Ff(\xi_x, \xi_y) = \int_{-\infty}^{\infty}\int_{-\infty}^{\infty} f(x, y)\exp(-j\xi_x x - j\xi_y y)dxdy, \tag{1.30}$$

$$f(x, y) = \frac{1}{4\pi^2}\int_{-\infty}^{\infty}\int_{-\infty}^{\infty} Ff(\xi_x, \xi_y)\exp(j\xi_x x + j\xi_y y)d\xi_x d\xi_y, \tag{1.31}$$

where $Ff(\xi_x, \xi_y)$ is the Fourier transform of $f(x, y)$, and $\boldsymbol{\xi} = (\xi_x, \xi_y)^T$ is the frequency coordinate in the Fourier domain; the superscript T is used for matrix or vector transpose and will be used throughout this book. A higher-dimension Fourier transform pair can be similarly defined. Fast Fourier transform (FFT) has been developed to accelerate the computing. Fourier transforms are vastly important and can be explored in more depth in Refs. 43 and 44. Fourier optics[67] is a good example of its tremendous applicability in optics.

A carrier fringe pattern can be written as

$$f(x, y) = a(x, y) + b(x, y)\cos[\varphi(x, y) + \omega_{cx}x + \omega_{cy}y] + n(x, y), \tag{1.32}$$

where $\boldsymbol{\omega}_c = (\omega_{cx}, \omega_{cy})^T$ denotes the spatial carrier frequency. Euler's formula is used:

$$\exp(j\eta) = \cos\eta + j\sin\eta, \tag{1.33}$$

where $j = \sqrt{-1}$. With Euler's formula, Eq. (1.32) can be rewritten as

$$\begin{aligned} f(x, y) = a(x, y) &+ c(x, y)\exp[j(\omega_{cx}x + \omega_{cy}y)] \\ &+ c^*(x, y)\exp[-j(\omega_{cx}x + \omega_{cy}y)] + n(x, y), \end{aligned} \tag{1.34}$$

where the superscript* indicates the conjugate of a complex number, and

$$c(x, y) = \frac{1}{2}b(x, y)\exp[j\varphi(x, y)]. \tag{1.35}$$

A 2D Fourier transform on Eq. (1.34) yields

$$\begin{aligned} Ff(\xi_x, \xi_y) = Fa(\xi_x, \xi_y) &+ Fc(\xi_x - \omega_{cx}, \xi_y - \omega_{cy}) \\ &+ Fc^*(\xi_x + \omega_{cx}, \xi_y + \omega_{cy}) + Fn(\xi_x, \xi_y)\ . \end{aligned} \tag{1.36}$$

In the Fourier domain, $Fa(\xi_x, \xi_y)$, $Fc(\xi_x - \omega_{cx}, \xi_y - \omega_{cy})$, and $Fc^*(\xi_x + \omega_{cx}, \xi_y + \omega_{cy})$ concentrate around $(0, 0)$, $(\omega_{cx}, \omega_{cy})$, and $(-\omega_{cx}, -\omega_{cy})$, respectively, while $Fn(\xi_x, \xi_y)$ usually permeates the entire Fourier domain. If the first three terms in the right side of Eq. (1.36) do not overlap with each other, the second term $Fc(\xi_x - \omega_{cx}, \xi_y - \omega_{cy})$ can be isolated and retained. If it is further shifted toward the origin, $Fc(\xi_x, \xi_y)$ is obtained. An inverse Fourier transform of $Fc(\xi_x, \xi_y)$ returns $c(x, y)$. The phase can then be extracted using Eq. (1.17) with $N(x, y) = \mathrm{Im}[c(x, y)]$ and $D(x, y) = \mathrm{Re}[c(x, y)]$, which are the imaginary and real parts of $c(x, y)$, respectively.

The success of the Fourier transform technique requires the first three terms in the right side of Eq. (1.36) to be separable. To fulfill this requirement, $Fa(\xi_x, \xi_y)$ and $Fc(\xi_x, \xi_y)$ should be band-limited, and the carrier frequency $\boldsymbol{\omega}_c$ should be high enough to drag the terms away from each other. The frequency band of $Fa(\xi_x, \xi_y)$ depends on $a(x, y)$ and is usually narrow according to the property of fringe patterns P1. The frequency band of $Fc(\xi_x, \xi_y)$ depends on both $b(x, y)$ and $\varphi(x, y)$. Since $b(x, y)$ varies slowly (P2), but $\varphi(x, y)$ can vary quickly (P3), the latter has a more significant and often dominating influence. When the carrier fringe pattern occurs densely in some regions and sparsely in others, the band of $Fc(\xi_x, \xi_y)$ is wide, making the isolation of $Fc(\xi_x, \xi_y)$ difficult. Even if $Fc(\xi_x, \xi_y)$ can be successfully isolated within its band, noise $Fn(\xi_x, \xi_y)$ survives, resulting in a noisy phase.

The phase-shifting and Fourier transform techniques can be linked. As shown in Eq. (1.18), the phase shifts can be seen as a temporal carrier so that the phase-shifted fringe patterns can be written as

$$\begin{aligned} f(x, y; t_k) = a(x, y) &+ b(x, y)\cos[\varphi(x, y) + \omega_{ct}t_k] \\ &+ n(x, y; t_k), \quad k = 0, \ldots, K - 1. \end{aligned} \tag{1.37}$$

For the example given in Section 1.3.2, we have $\omega_{ct} = \pi/2$, $t_k = k$, $K = 4$. A 1D Fourier transform along the time axis is applied to Eq. (1.37). Since all quantities, $a(x, y)$, $b(x, y)$, and $\varphi(x, y)$, are time-invariant, $Fa(x, y; \xi_t)$, $Fc(x, y; \xi_t - \omega_{ct})$, and $Fc^*(x, y; \xi_t + \omega_{ct})$ are all delta functions. Thus, we have

$$Fc(x, y; \xi_t - \omega_{ct}) = Ff(x, y; \xi_t)\delta(\xi_t - \omega_{ct}). \tag{1.38}$$

With the definition of Fourier transform in Eq. (1.28), we have

$$Fc(x, y; \xi_t - \omega_{ct}) = \left[\sum_{k=0}^{3} f(x, y; t_k)\exp(-j\omega_{ct}t_k)\right]\delta(\xi_t - \omega_{ct}), \tag{1.39}$$

which can be expanded as

$$\begin{aligned} Fc(x, y; \xi_t - \omega_{ct}) = \big\{&\big[f(x, y; t_0) - f(x, y; t_2)\big] \\ &+ j\big[f(x, y; t_3) - f(x, y; t_1)\big]\big\}\delta(\xi_t - \omega_{ct}). \end{aligned} \tag{1.40}$$

After it is shifted toward the origin and undergoes an inverse Fourier transform, we have

$$c(x, y) = [f(x, y; t_0) - f(x, y; t_2)] + j[f(x, y; t_3) - f(x, y; t_1)], \tag{1.41}$$

whose imaginary part and real part correspond exactly to Eqs. (1.15) and (1.16), respectively, but are obtained from a different manner. The link between the two techniques is explored in Ref. 68 and utilized, for example, in Ref. 69 to convert from phase shifting to Fourier transform, and alternately in Ref. 70 to convert from Fourier transform to phase shifting.

1.5 Phase Unwrapping

The significance of the phase-shifting and Fourier transform techniques is that they successfully solve the first two difficulties in fringe pattern analysis—ill-posedness (D1) and sign ambiguity (D2). However, the third difficulty—order ambiguity (D3)—remains. As can be seen from Sections 1.3 and 1.4, in both techniques, the phase is calculated using Eq. (1.17), which can only give the principle value of the arctangent function. We start from the noiseless case, which yields $\varphi_w(x, y) \in (-\pi, \pi]$ from Eq. (1.17). Removing the order ambiguity and recovering $\varphi(x, y)$ from $\varphi_w(x, y)$ is called phase unwrapping.

The relationship between $\varphi_w(x, y)$ and $\varphi(x, y)$ is as simple as

$$\varphi(x, y) = \varphi_w(x, y) + 2k(x, y)\pi, \quad k(x, y) \in \mathbf{Z}, \tag{1.42}$$

which shows that to unwrap the phase is to determine $k(x, y)$. In the following, $\varphi(x, y)$ is assumed to have spatial continuity, which is stronger than piecewise continuity in P3. We assume that the pixel (x_{i-1}, y_{i-1}) has already been unwrapped, with a result of $\varphi(x_{i-1}, y_{i-1})$. Its neighboring pixel (x_i, y_i) is

to be unwrapped from $\varphi_w(x_i, y_i)$. Since the phase is continuous, if the sampling is dense enough in space, we have

$$-\pi < \varphi(x_i, y_i) - \varphi(x_{i-1}, y_{i-1}) < \pi. \tag{1.43}$$

By incorporating Eq. (1.42), this inequality can be rewritten as

$$-\pi < \varphi_w(x_i, y_i) + 2k(x_i, y_i)\pi - \varphi(x_{i-1}, y_{i-1}) < \pi, \tag{1.44}$$

which can be rearranged as

$$-0.5 + \frac{\varphi(x_{i-1}, y_{i-1}) - \varphi_w(x_i, y_i)}{2\pi} < k(x_i, y_i) < 0.5 + \frac{\varphi(x_{i-1}, y_{i-1}) - \varphi_w(x_i, y_i)}{2\pi}. \tag{1.45}$$

This relationship corresponds to the round function,

$$k(x_i, y_i) = \text{round}\left[\frac{\varphi(x_{i-1}, y_{i-1}) - \varphi_w(x_i, y_i)}{2\pi}\right], \tag{1.46}$$

where round$(\cdot)$ rounds a decimal to its nearest integer. To summarize, the phase can be unwrapped as

$$\varphi(x_i, y_i) = \varphi_w(x_i, y_i) + \text{round}\left[\frac{\varphi(x_{i-1}, y_{i-1}) - \varphi_w(x_i, y_i)}{2\pi}\right] \cdot 2\pi. \tag{1.47}$$

Although theoretically viable and simple, phase unwrapping is challenging in practice due to noise (D4) and phase discontinuities (D5). If noise occurs, the determination of $k(x_i, y_i)$ in Eq. (1.46) can be wrong. If one pixel goes wrong, the subsequent pixels are unlikely to return to the right track. In an invalid region, the light field is weak, and the extracted phase is noisy. This case can thus be treated as a noise problem in phase unwrapping. Phase discontinuities can be classified into two categories. The first is caused by the order ambiguity in phase extraction that uses an arctangent function. These are "pseudo-phase discontinuities" and are removed by phase unwrapping. The second is encountered when the physical quantities being measured are discontinuous, for example, when the profile of an object being measured has staircases, or when there are multiple disjoined objects. "True phase discontinuities" result and are difficult to tackle.[71] The most successful techniques for solving the "true-phase discontinuities" include the temporal phase-unwrapping technique, which assumes that the phase is temporally continuous and obtains the continuous phase by accumulating phase difference between consecutive frames,[72] and the multifrequency technique, which generates a long synthetic wavelength.[73,74] Phase unwrapping has been an active topic for decades. Many good algorithms have been proposed to meet the challenges.[4,75,76]

1.6 Fringe Pattern Classification

Based on the above introduction, the fringe patterns modeled in Eq. (1.9) are further classified into four types. All of these types of fringe patterns can be equipped with a time axis to make them a sequence of dynamic fringe patterns.

1.6.1 Exponential phase fields

In both phase-shifting and Fourier transform techniques, the phase is extracted by Eq. (1.17). By treating $D(x, y)$ and $N(x, y)$ as the real and imaginary parts, respectively, a complex field $D(x, y) + jN(x, y)$ can be constructed as the first type of fringe pattern:

$$\text{(T1)} \quad f(x, y) = b(x, y)\exp[j\varphi(x, y)] + n(x, y). \tag{1.48}$$

This is called an exponential phase field (EPF) throughout the book. It is also called a phasor.[77] In the Fourier transform technique, the term $c(x, y)$ is naturally an EPF. Although $\varphi_w(x, y)$ is not continuous, its EPF is continuous because $\exp[j\varphi_w(x, y)] = \exp[j\varphi(x, y)]$. Processing an EPF is preferable to processing a wrapped phase map.

1.6.2 Wrapped phase maps

A wrapped phase map is the angle of an EPF. Wrapped phase maps need to be processed and unwrapped, and are considered the second type of fringe pattern. By reasonably assuming that $n_\varphi(x, y) \in (-\pi, \pi]$, the left side of Eq. (1.17) can be rewritten as $\varphi_w(x, y) + n_\varphi(x, y) + 2k\pi$, $k \in \{-1, 0, 1\}$. Thus, we model the second type of fringe pattern as

$$\text{(T2)} \quad f(x, y) = \varphi_w(x, y) + n(x, y). \tag{1.49}$$

A phase difference map between two speckle fields can be either extracted from the speckle correlation fringe patterns given in Eq. (1.7), or directly formed from two measured speckle phases.[78] A T2 fringe pattern can be easily converted to T1 with $b(x, y) = 1$.

1.6.3 Carrier fringe patterns

A carrier fringe pattern is the third type of fringe pattern:

$$\text{(T3)} \quad f(x, y) = a(x, y) + b(x, y)\cos[\varphi(x, y) + \omega_{cx}x + \omega_{cy}y] + n(x, y). \tag{1.50}$$

It can also be converted to T1 through forward and inverse Fourier transforms, as discussed in Section 1.4.

1.6.4 Single closed fringe patterns

A fringe pattern without a temporal or spatial carrier cannot be easily converted to T1. As no carrier is presented, the fringe patterns are closed. These are classified as the fourth type of fringe pattern:

$$\text{(T4)} \quad f(x, y) = a(x, y) + b(x, y)\cos[\varphi(x, y)] + n(x, y). \tag{1.51}$$

1.7 Fringe Pattern Simulation

Simulated fringe patterns are useful to quantitatively evaluate the effectiveness of an algorithm. Experimental fringe patterns, on the other

hand, are often used for qualitative and visual judgment, as they often lack the ground truth data. Both simulated and experimental fringe patterns are necessary in algorithm evaluation. Fringe patterns can be easily simulated according to Eqs. (1.48)–(1.51) and the fringe properties P1–P4. Additive noise is often modeled as white Gaussian noise. Speckle noise should also be considered.

A speckle correlation fringe pattern can be simulated simply according to Eqs. (1.7) and (1.8) with the following settings: $a_r^2(x, y; t) = 1$; $a_o^2(x, y; t)$ is a random variable with a negative exponential distribution; $\varphi_o(x, y; t_0)$ is uniformly distributed in $(-\pi, \pi]$; $\Delta\varphi_o(x, y; t_0, t)$ is (piecewise) smooth; and $\varphi_r(x, y) = 0$.[79] By this simulation the speckle radius is 1 pixel, and the speckle diameter is 2 pixels, which means that the speckle (one period of waving intensity, from bright to bright or from dark to dark) is sampled by 2 pixels, which minimally satisfies the Nyquist sampling requirement.[43–44]

Another method for speckle simulation is to mimic a $4f$ system to manipulate the spectrum of light field.[80] A low-pass filter $L(\xi_x, \xi_y)$ is applied to the object beams to mimic an aperture,

$$A_o(x, y; t) = F^{-1}\big(F\{a_o(x, y; t)\exp[j\varphi_o(x, y; t)]\}L(\xi_x, \xi_y)\big), \qquad (1.52)$$

where $F(\cdot)$ and $F^{-1}(\cdot)$ are forward and inverse Fourier transforms, respectively; $\varphi_o(x, y; t)$ is a random variable uniformly distributed in $(-\pi, \pi]$; and $a_o(x, y; t) = 1$ is set to all t for simplicity. Similarly, the reference beam $A_r(x, y; t) = 1$ is set to all t for simplicity. Two speckle fields $I(x, y; t_0)$ and $I(x, y; t)$ at time instances t_0 and t, respectively, are simulated according to Eq. (1.3). Between these two time instances, the phase change $\Delta\varphi_o(x, y; t_0, t)$ is (piecewise) smooth. A speckle correlation fringe pattern, $I_c(x, y; t_0, t)$, is generated according to Eq. (1.6). The absolute difference as a speckle correlation fringe pattern $I_c(x, y; t_0, t) = |I(x, y; t) - I(x, y; t_0)|$ is also a frequently used option. The following circle is a possible design of the low-pass filter $L(\xi_x, \xi_y)$ that can be used to generate speckle with a radius of r_s pixels in an image with a size of $N_x \times N_y = N \times N$:

$$L(\xi_x, \xi_y) = \begin{cases} 1, & \xi_x^2 + \xi_y^2 \le \left(\dfrac{N}{2r_s}\right)^2 \\ 0, & \text{otherwise.} \end{cases} \qquad (1.53)$$

When r_s increases, the aperture size decreases, and more high-frequency components are blocked, resulting in a larger speckle size. The minimum speckle radius is 1 pixel.

Two phase distributions with a size of $N_x \times N_y = N \times N$ are used for demonstrations in this book. The first phase distribution is quadratic and symmetrical, thus simple, but not uncommon:

$$\varphi(x, y) = 0.5\kappa\big[(x - N/2)^2 + (y - N/2)^2\big], \quad 1 \le x, y \le N, \qquad (1.54)$$

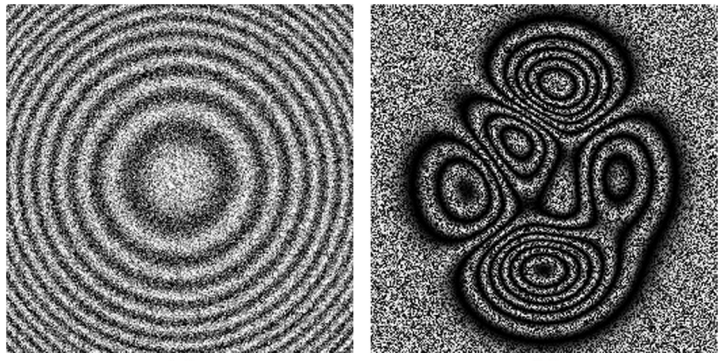

Figure 1.2 Simulated fringe patterns (a) with the circular phase and additive noise, and (b) with the peaks phase and speckle noise.

where the parameter κ is used to control fringe density. This is called the circular phase. The second phase distribution contains several peaks and is more complicated:

$$\varphi(x, y) = \kappa \cdot \text{peaks}(N), \tag{1.55}$$

where the parameter κ is again used to control fringe density, and peaks(N) is a built-in MATLAB® function that uniformly samples $N \times N$ points from the following surface:

$$z(x, y) = 3(1-x)^2\exp\left[-x^2-(y+1)^2\right] - 10(x/5 - x^3 - y^5)\exp(-x^2-y^2) - \frac{1}{3}\exp\left[-(x+1)^2 - y^2\right], -3 \le x, y \le 3\ . \tag{1.56}$$

This is called the "peaks phase."

A fringe pattern with $a(x, y) = b(x, y) = 1$ and the circular phase ($\kappa = 0.005$) is shown in Fig. 1.2(a). Additive noise with mean of zero and standard deviation of 1 is added. A fringe pattern with the peaks phase ($\kappa = 5$) is shown in Fig. 1.2(b). The speckle noise with radius of 1 is simulated.

1.8 Windowed Fringe Pattern Analysis

In most optical measurement, a point in a field undergoing measurement has nothing to do with a point far away, but it is likely similar to a point nearby. This local similarity is helpful in suppressing noise and estimating parameters. Many algorithms indeed process a fringe pattern in a block-by-block (or window-by-window) manner. We call this windowed fringe pattern analysis. Nonlocal algorithms[81,82] are not the focus of this book.

In one extreme, the phase-shifting technique works in a small 1D window along the t axis. Since the window is small and only one pixel every few frames

is involved, a strong assumption for parameters can be made: the phase, the background, and the fringe amplitude are all constant in different frames. Because of this assumption, the phase can be easily retrieved. However, a small window cannot sufficiently suppress the noise since only a few frames are involved for each pixel. In the other extreme, the 2D Fourier transform technique works in the largest window—the entire frame. Only the weak assumption that the phase is band-limited can be made. Although many pixels are involved, this technique does not guarantee sufficient noise suppression and is largely influenced by the frequency bandwidth of $Fc(\xi_x, \xi_y)$. For example, in Eq. (1.36), if each of $Fc(\xi_x - \omega_{cx}, \xi_y - \omega_{cy})$ and $Fc^*(\xi_x + \omega_{cx}, \xi_y + \omega_{cy})$ occupies half of the Fourier domain, when $Fc(\xi_x - \omega_{cx}, \xi_y - \omega_{cy})$ is isolated and retained, half of the noise energy will survive.

The question is whether a medium-sized window produces better results. Mean and median filters are good examples.[83] Unfortunately, they do not work well for waving structures in fringe patterns. A good exception is the sine/cosine filter,[84] but it fails to deal with fringe patterns with fast waving structures.[85] The waving structure in a fringe pattern is mainly caused by the phase. Since the phase is smooth, at least piecewise (fringe property P3), near a point (u, v) it can be expanded into the Taylor series,[86]

$$\varphi(x, y) \approx \sum_{n=0}^{N_\varphi} \left\{ \frac{1}{n!} \left[(x-u)\frac{\partial}{\partial x} + (y-v)\frac{\partial}{\partial y} \right]^n \varphi(u, v) \right\}, \tag{1.57}$$

where N_φ is the order of the expanded polynomial, $n!$ denotes the factorial of n, $\partial/\partial x$, $\partial/\partial y$ are partial differentiations with respect to x and y respectively, and the partial differentiations are applied to $\varphi(x, y)$ and evaluated at (u, v). The phase can thus be approximated locally as a polynomial. For example, the phase can be assumed to be constant ($N_\varphi = 0$), linear ($N_\varphi = 1$), or quadratic ($N_\varphi = 2$), etc. A smaller N_φ indicates a stronger assumption, which is suitable in a smaller window. Based on these assumptions, various algorithms have been developed to analyze fringe patterns. These algorithms, such as spin filters (constant phase), regularized phase tracking (linear phase), and windowed Fourier transform (quadratic phase), will be explored in this book. Noise is sufficiently suppressed using these techniques, making phase unwrapping and fringe demodulation much easier. The Taylor expansion in Eq. (1.57) is 2D, but it can be extended to 1D or higher dimensions.

The phase extracted by windowed fringe pattern analysis may present some ambiguities, due to the nature of optical interferometry. A well-known example is the phase-order ambiguity, which can be removed by phase unwrapping where phase continuity is enforced. The other is sign ambiguity and can be removed by forcing the continuity of local frequency. "Continuity" is defined by derivatives, which are the relationships between neighboring

points. Thus, the natural process of removing the ambiguity begins at a seed pixel, moves to its neighbor, and then to the neighbor's neighbor, until all of the pixels are processed. In this way, the processing footprint forms a path. Among many possible paths, one reasonable option is to follow the decrease of pixel quality. The high-quality pixels are processed first, followed by low-quality pixels, so that if there is an error or failure, it is postponed. This is called quality guidance. To combine the above two important concepts, namely, windowed fringe pattern analysis and quality guidance, most algorithms in this book are quality-guided windowed fringe pattern analysis. We use the term windowed fringe pattern analysis to serve as a concise book title with the understanding that quality guidance naturally follows.

A window isolates a patch of fringe pattern for analysis. There are many window functions,[87] among which, rectangular and Gaussian windows are the most extensively used throughout this book. A rectangular window treats the data in the window equally. It fully utilizes the data information and is the most economical. It is always used when the window size has to be small. Take a 1D rectangular window as an example. Its window size is denoted as N_{wx}, covering $[-N_{wx}/2, N_{wx}/2]$ for a continuous window in theoretical analysis, and $[-(N_{wx}-1)/2, (N_{wx}-1)/2]$ for a discrete window in algorithm development. For a discrete window, the window size N_{wx} is an odd number.

A Gaussian window has higher emphasis on the data near the window center and lower emphasis on the data further away from the window center. This is reasonable because the data in the center are usually more trustworthy. A Gaussian window is often selected when the window size can be luxuriously large.

For a continuous signal $f(x)$, its L^p norm is defined as follows:[88]

$$\|f\|_p = \left(\int_{-\infty}^{\infty} |f(x)|^p\right)^{\frac{1}{p}}. \tag{1.58}$$

All signals with finite L^p norm form a space $L^p(\mathbf{R})$. For a window $g_x(x)$, $\|g_x\|_1$ signifies the area under $g_x(x)$, and $\|g_x\|_2$ emphasizes the energy of $g_x(x)$. A Gaussian window, with $\|g_x\|_1 = 1$, and its Fourier spectrum, are

$$g_x(x) = \frac{1}{\sqrt{2\pi}\sigma_x}\exp\left(-\frac{x^2}{2\sigma_x^2}\right), \tag{1.59}$$

$$Fg_x(\xi) = \exp\left(-\frac{\sigma_x^2\xi^2}{2}\right). \tag{1.60}$$

A Gaussian window, with $\|g_x\|_2 = 1$, and its Fourier spectrum, are

$$g_x(x) = \left(\pi\sigma_x^2\right)^{-\frac{1}{4}}\exp\left(-\frac{x^2}{2\sigma_x^2}\right), \tag{1.61}$$

and $$Fg_x(\xi) = \left(4\pi\sigma_x^2\right)^{\frac{1}{4}} \exp\left(-\frac{\sigma_x^2\xi^2}{2}\right). \tag{1.62}$$

The Gaussian window is symmetrical, namely, $g_x(-x) = g_x(x)$. Note that the coordinate x is emphasized, but it can be replaced by other coordinates. For example, $g_y(y)$ can be defined in the same way but along the y axis. A 2D Gaussian window can be constructed as

$$g(x, y) = g_x(x)g_y(y), \tag{1.63}$$

which is called separable. Discrete windows can be obtained by sampling the continuous counterparts. The l^p norm should be used, and is defined in the same way as Eq. (1.58), except that the integration is replaced by summation. All of the signals with finite l^p norm form a space $l^p(\mathbf{Z})$. We generally call σ_x a Gaussian window size, with the understanding that the actual window size is $N_{wx} = \infty$ [covering $(-\infty, \infty)$] for a continuous window in theoretical analysis and $N_{wx} = 2t\sigma_x + 1$ (covering $[-t\sigma_x, t\sigma_x]$) for a discrete window in algorithm development, where $t = 3$ is a safe choice and $t = 2$ is also frequently used to shorten the window with minimal information loss.

We must mention that the phase $\varphi(x, y)$ can be discontinuous (D5). If this happens, both the Taylor expansion in Eq. (1.57) for windowed fringe pattern analysis and the continuity assumption for quality guidance are no longer reasonable. As a consequence, the quality-guided windowed fringe pattern analysis algorithms discussed in this book are usually very successful for cases of continuity but may not be for cases of discontinuity.[89] However, because these algorithms respond differently to the continuous and discontinuous regions, they can usually be used to differentiate regions or detect boundaries between the regions, even with the presence of the discontinuity problem.

We link the windowed fringe pattern analysis to the sparse and redundant representations that are under intensive study in the signal and image processing community.[90] Excellent algorithms have been developed in this direction. For example, the BM3D[91] can denoise a fringe pattern with very good results. Interested readers will find that the algorithms developed in this book also embody the spirit of sparsity and redundancy. These algorithms can achieve outstanding performance because they enable precise modeling of fringe patterns; thus, a perfect dictionary for fringe pattern representation can be easily built. The importance of a data model is highlighted in Ref. 92.

Finally, the windowed fringe pattern analysis can be linked to another important optical measurement method, digital image correlation (DIC).[93,94] In DIC, the displacement of each image patch in the first image is determined by finding its most similar patch in the second image. Thus, DIC performs a windowed correlation analysis. Because the final correlation result of one patch is usually used as the initial guess for the next patch in the DIC implementation, quality guidance can play a role in path selection.[95] Since

DIC does not have the ambiguity problems associated with fringe pattern analysis, and the noise is often light, the requirement for quality guidance is not as demanding as in fringe pattern analysis. Interested readers can refer to Ref. 96 for more information.

1.9 Book Organization

This book is organized by three interweaving threads. The first is the quality-guided windowed fringe pattern analysis, which is the overarching theme of the book and applies to all of the chapters. The second thread forms the main structure by explaining how to process different types of fringe patterns according to their respective features—exponential phase fields (Chapters 2 and 3), wrapped phase maps (Chapter 4), carrier fringe patterns (Chapter 5), closed fringe patterns (Chapters 6 and 7), and a sequence of dynamic fringe patterns (Chapter 8) are all explored. The third thread covers the A3 requirements for fringe pattern analysis algorithms. These requirements are discussed throughout Chapters 2–8. In addition, Chapter 9 is dedicated to acceleration through computing hardware.

References

1. A. K. Asundi, *MATLAB® for Photomechanics: A Primer*, Elsevier, The Netherlands (2002).
2. D. W. Robinson, "Automatic fringe analysis with a computer image-processing system," *Appl. Opt.* **22**, 2169–2176 (1983).
3. G. T. Reid, "Automatic fringe pattern analysis: a review," *Optics and Lasers in Engineering* **7**, 37–68 (1986).
4. D. W. Robinson and G. T. Reid, Eds., *Interferogram Analysis*, Institute of Physics Publishing, Bristol (1993).
5. J. M. Huntley, "Automated fringe pattern analysis in experimental mechanics: a review," *Journal of Strain Analysis* **33**, 105–125 (1998).
6. M. Kujawińska and W. Osten, "Fringe pattern analysis methods: up-to-date review," *Proc. SPIE* **3407**, 56–66 (1998).
7. B. V. Dorrío and J. L. Fernández, "Phase-evaluation method in whole-field optical measurement techniques," *Meas. Sci. Technol.* **10**, R33–R55 (1999).
8. M. Servin and M. Kujawinska, "Modern fringe pattern analysis in interferometry," D. Malacara and B. J. Thompson, Eds., Chapter 12 in *Handbook of Optical Engineering*, Marcel Dekker, New York, pp. 373–426 (2001).
9. M. Hipp, J. Woisetschläger, P. Reiterer, and T. Neger, "Digital evaluation of interferograms," *Measurement* **36**, 53–66 (2004).